nature neuroscience

SUPPLEMENTARY INFORMATION

https://doi.org/10.1038/s41593-019-0523-z

In the format provided by the authors and unedited.

Memory retrieval modulates spatial tuning of single neurons in the human entorhinal cortex

Salman E. Qasim[1], Jonathan Miller[1], Cory S. Inman[2], Robert E. Gross[2], Jon T. Willie[2], Bradley Lega[3], Jui-Jui Lin[3], Ashwini Sharan[4], Chengyuan Wu[4], Michael R. Sperling[5,6], Sameer A. Sheth[7], Guy M. McKhann[8], Elliot H. Smith[9], Catherine Schevon[10], Joel M. Stein[11] and Joshua Jacobs[1]*

[1]Department of Biomedical Engineering, Columbia University, New York, NY, USA. [2]Department of Neurological Surgery, Emory University, Atlanta, GA, USA. [3]Department of Neurological Surgery, University of Texas Southwestern, Dallas, TX, USA. [4]Department of Neurological Surgery, Thomas Jefferson University, Philadelphia, PA, USA. [5]Department of Neurology, Thomas Jefferson University, Philadelphia, PA, USA. [6]Jefferson Comprehensive Epilepsy Center, Jefferson University Hospitals, Philadelphia, PA, USA. [7]Department of Neurological Surgery, Baylor College of Medicine, Houston, TX, USA. [8]Department of Neurological Surgery, Columbia University, New York, NY, USA. [9]Department of Neurosurgery, University of Utah, Salt Lake City, UT, USA. [10]Department of Neurology, Columbia University, New York, NY, USA. [11]Department of Radiology, University of Pennsylvania, Philadelphia, PA, USA.
*e-mail: joshua.jacobs@columbia.edu

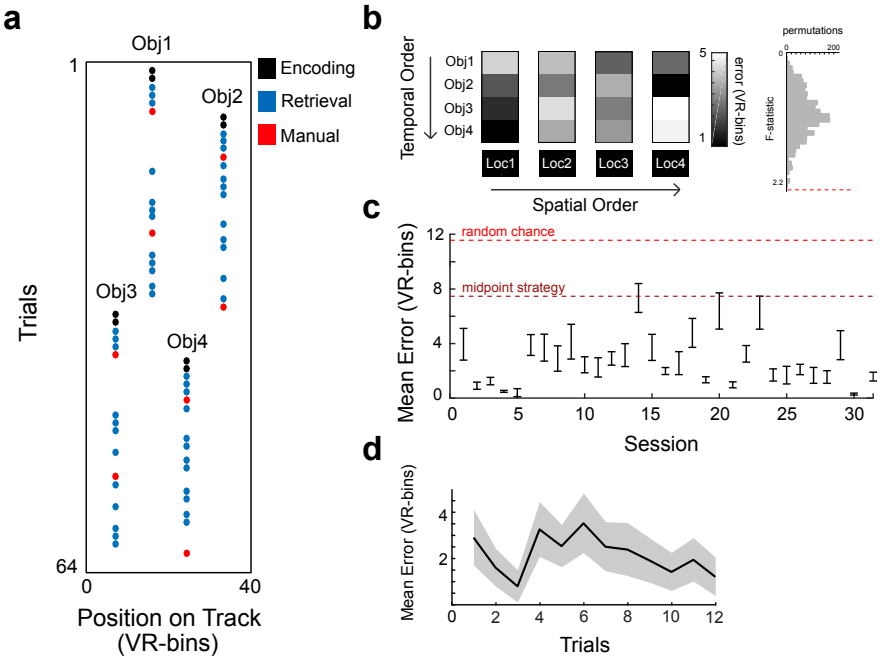

Supplementary Figure 1: **Trial structure and behavioral performance.** a) Schematic depicting the trial structure of the task for one example session. The first two trials for each object cue were encoding trials (black), followed by retrieval trials (passive movement, blue; manual movement, red). The cued object switched between objects 1 and 2 during the first half of the task and between objects 3 and 4 for the second half. Across sessions, the trials selected for each cue were random. b) Left: Error plotted as a function of both temporal order and spatial order of objects. Darker colors indicate lower error. Columns represent effect of spatial order, rows represent effect of temporal order, individual bins represent interaction between specific spatial and temporal ordering on shuffled error from ANOVA. Right: Analysis of effects of temporal and spatial order. Because our task design dissociated the spatial and temporal order that cued objects appeared in, we used an ANOVA to compute the effects of the objects' spatial (columns) and temporal (rows) order and their interaction, on subjects' distance error. We found a significant interaction ($F_{(9,\ 1385)} = 2.25$, $p < 10^{-3}$, permutation test) such that certain combinations of spatial and temporal order led to differences in performance. Red dotted line indicates true test statistic and the histogram indicates the distribution of permuted interaction test statistics for effects of temporal and spatial order on shuffled error. Analyses performed on 1416 retrieval trials across 31 sessions. c) Mean error for each session ($n = 48$ trials for 28 full sessions, 24 for 3 truncated sessions). Error bars indicate SEM, and center of bars indicates mean. Red dotted lines indicate the error levels expected by chance, following strategies where the subjects respond randomly (light red) and where the subject always responds at the midpoint of the environment (dark red). In 30 of 31 sessions, the subject's mean error was below both of these chance levels, indicating that subjects reliably performed the task well. d) Mean error across the 12 retrieval trials (dots in panel *A*) comprising each object–cue block, averaged over subjects ($n = 118$ trial blocks over 31 sessions). Shading indicates SEM. Note that subjects learned the object–location association quickly (first two trials), only to show increased errors beginning after trial 3 upon the introduction of another object location to hold in memory.

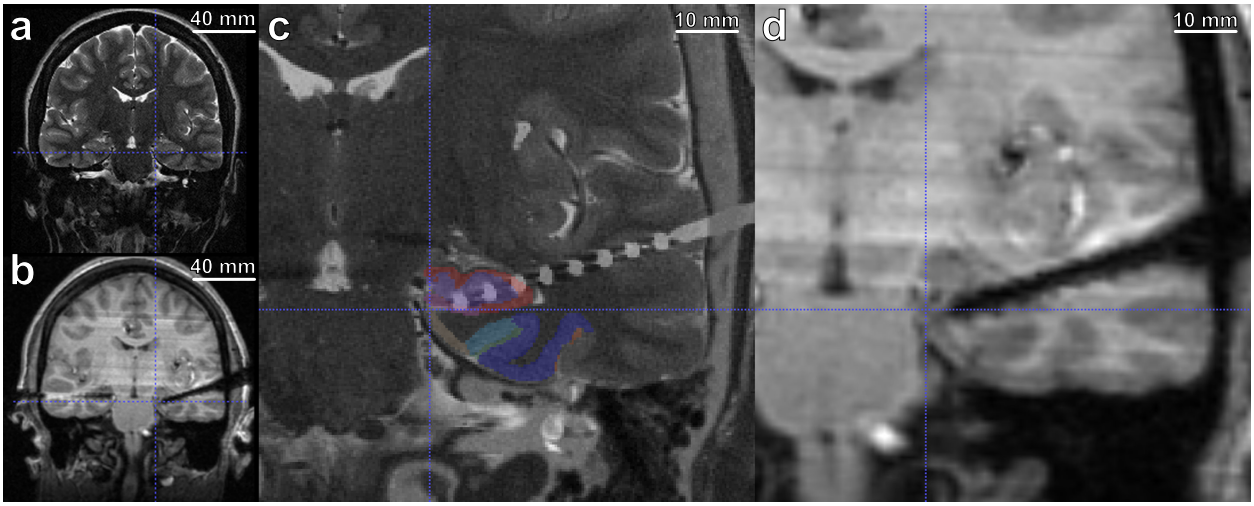

Supplementary Figure 2: **Approach to localization of microelectrodes.** a) Pre-implantation coronal T2-weighted MRI scan from one subject. b) Co-registered post-implantation T1-weighted MRI scan. c) Coronal T2 scan overlaid with software segementation of medial-temporal subregions and the post-implantation CT to show macroelectrodes. crosshairs indicates the location of the microwires. Coloring scheme for the MTL segmentation: EC (tan), BA35 (light), BA36 (dark), subiculum (pink), dentate gyrus (purple), CA1 (red). d) Post-implantation 3D T1-weighted MRI showing the confirmed location of the micro-electrode from panel C (crosshairs) in EC.

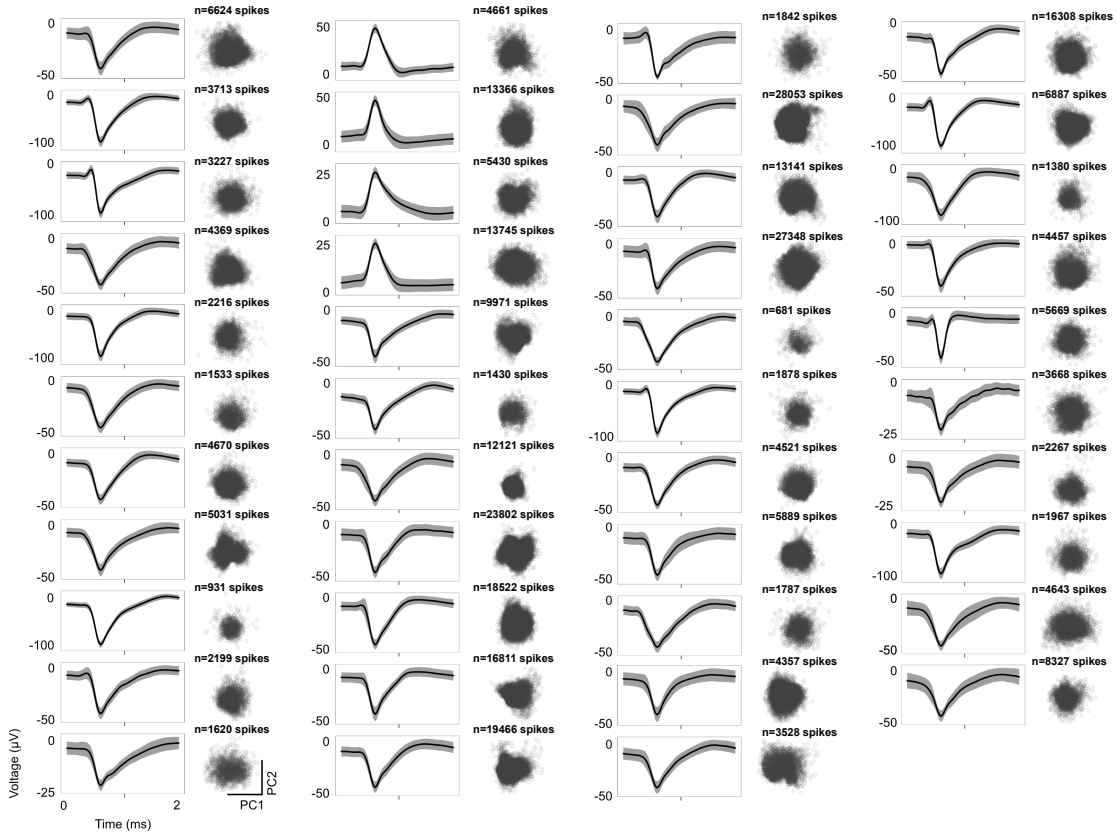

Supplementary Figure 3: **Memory-trace cell waveforms.** Each pair of plots depicts putative single-unit waveforms and their first two PCA components. Left panel: Mean single-unit waveform. Cells with positive polarity waveforms were recorded using the Neuralynx Cheetah system (see *Methods*). Shading indicates SEM. Right: Single clusters depicting first two principal components of each putative single-unit waveform. Spike number indicates the number of waveforms in each isolated single-unit depicted.

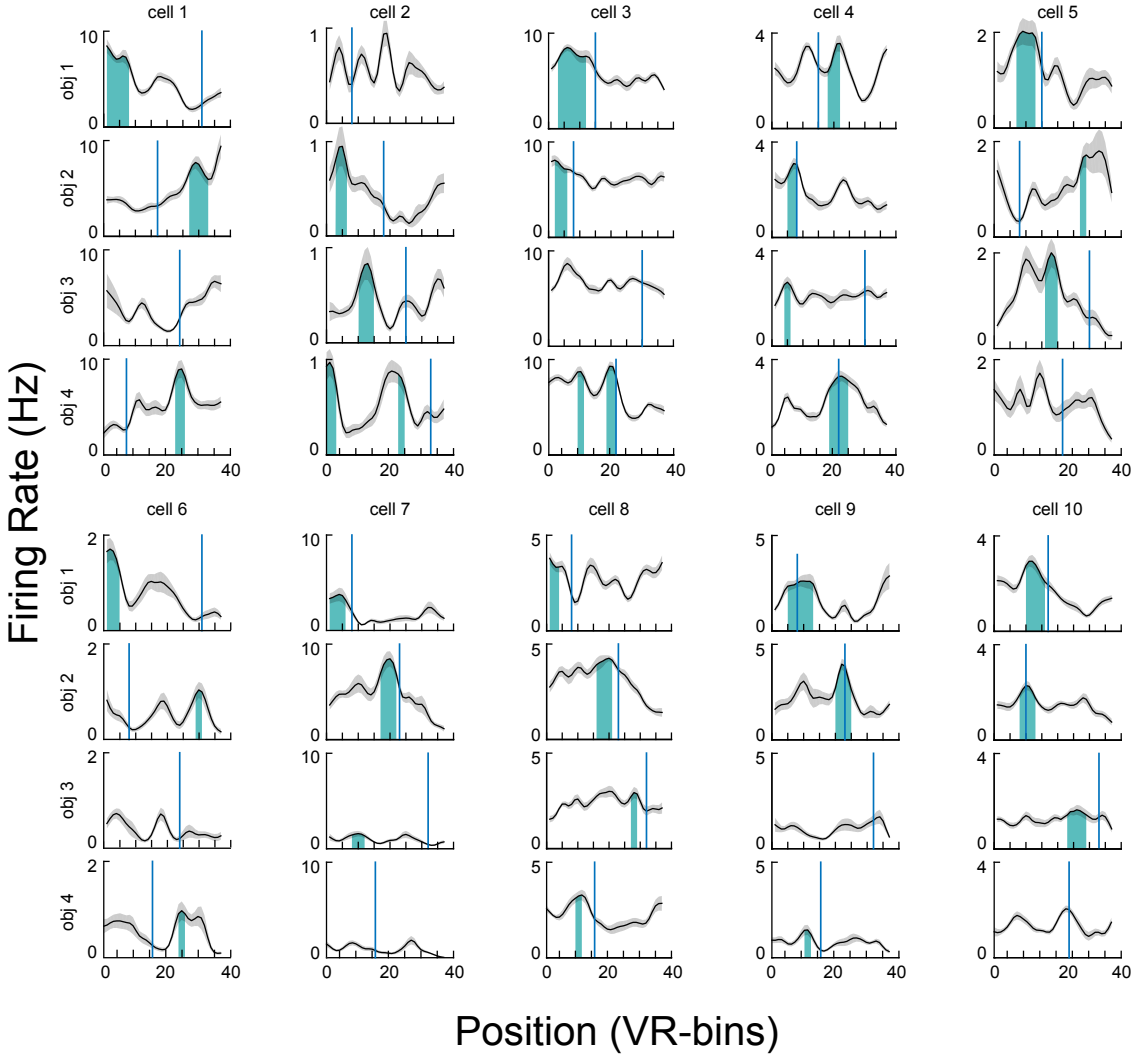

Supplementary Figure 4: **Examples of memory-trace cell activity during retrieval trials.** Plots illustrate mean firing rates of memory-trace cells for each object cue, as in Fig. 2b. Vertical lines indicate the location of the cued object, which was not visible to the subject during retrieval. Teal shading regions indicate spatial fields, identified as contiguous bins exceeding a non-parametrically determined threshold (see *Methods*). Grey shading indicates standard error ($n = 12$ trials). Regions: cells 1–2 = amygdala, cells 3–5 = EC, cell 6 = cingulate, cells 7–9 = EC, cell 10 = hippocampus.

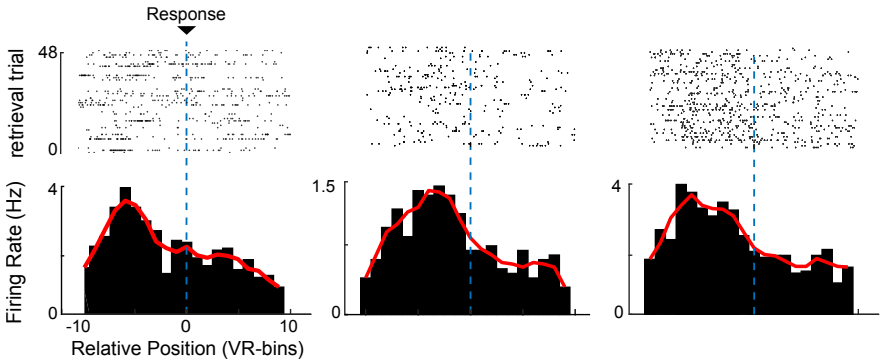

Supplementary Figure 5: **Memory-trace cell spiking relative to response location.** Raster plot of spiking activity and corresponding peristimulus histogram (PSTH) for three example EC memory-trace cells, aligned relative to response location (indicated by dotted line). Red line indicates smoothed mean firing rate.

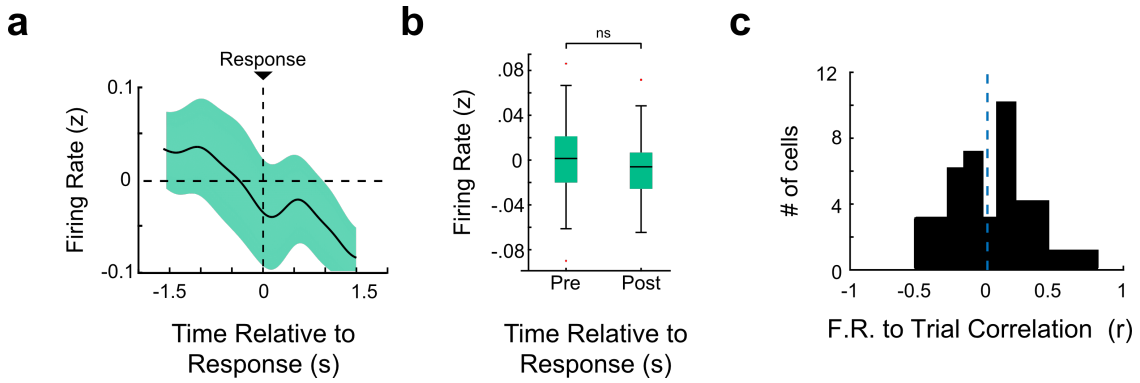

Supplementary Figure 6: **Memory-trace cell activity and time.** a) Mean firing rate (z-scored) of all memory-trace cells aligned to response time (black line, $n = 1990$ trials). This analysis used a 3-s window surrounding the response, as anticipatory motor responses occur within 1 s of a movement. Shading indicates SEM. Here, no bins showed significant difference from baseline, in contrast to our earlier analyses that showed significnat differences when we aligned neuronal activity as a function of spatial distance to the response (cf. Fig. 5b). This indicates that memory-trace cell activity likely does not reflect a time-locked anticipatory signal for the subjects' motor action, the button press. b) Memory-trace cell firing rate ($n = 43$) averaged in fixed time bins in the 3-s window from panel A (1.5-s pre- and 1.5-s post-response). Center line indicates median, box limits indicate interquartile range (IQR), whiskers indicate 1.5×IQR ($n = 1990$ trials). Circles indicate outliers. Label "ns" indicates $p > 0.05$ ($t(42) = 1.39$, $p = 0.17$ two-sided paired t test), which supports the result from Panel A that showed no significant difference between mean firing rates when binning by time. c) Histogram of Pearson's correlation coefficients testing the relation between memory-trace-cell firing rate and trial number within each session. This distribution did not significantly differ from zero ($t(42) = 0.74$, $p = 0.46$, two-sided t test), indicating that memory-trace-cell activity did not trend systematically over the course of a session.

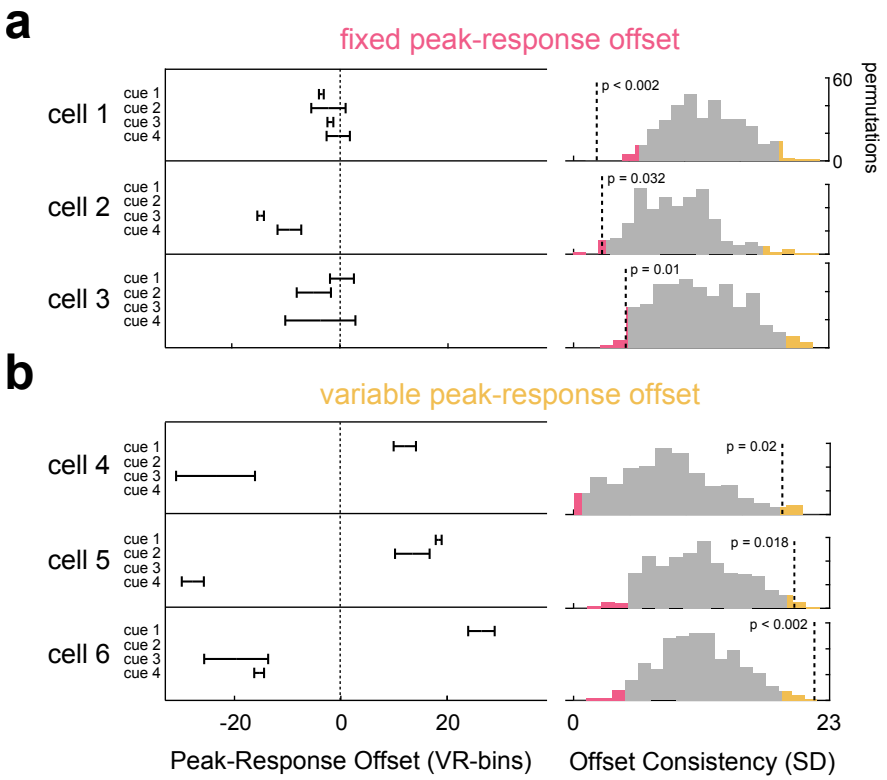

Supplementary Figure 7: **Example memory-trace cells that activated at consistent and variable offsets across cues.** a) The activity of three example cells that activated at consistent offsets relative to cues. Left: The spatial offsets between trace-field peaks and response location for different cues. Note that each cell had a trace-field for between one and four of the cues. Right: Analysis of offset consistency, parameterized by the standard deviation (SD) of peak-response offsets across cues. Histogram depicts distribution of SD measured from randomly shuffled data for each cell; black dotted line depicts true SD. Gray bins denote the center 95th percentile of permuted values. p value for each cell is labeled on the corresponding histogram relative to the shuffled data. This analysis was performed by identifying, for each cell, the peak-response offsets, or the distance between the trace-field peak and the response location, for all cues ($n = 48$ trials for 28 full sessions, 24 for 3 half sessions). We then computed the standard deviation (SD) of these offsets for each cell. A cell that activated at consistent offsets would show a small SD and, inversely, a cell that activated at variable offsets would have a large SD. To determine if a cell's SD value was *significantly* low or high, we compared the cell's actual SD with the distribution of SD values from a permutation procedure that was separately performed for each cell. We generated 500 surrogate values for each cell in a manner that matched the original data by following these steps: 1) determined which cues (1–4) the cell exhibited a field for, 2) generated a surrogate cell which had fields for the same cues by randomly selecting trace-fields for those cues from other memory-trace cells, 3) computed the standard deviation across the surrogate cell's peak-response offsets, 4) and repeated 500 times. Cells with SD values that were lower than 2.5% of the surrogate distribution were considered to fire at consistent offsets, and cells with SD values greater than 97.5% of the surrogate distribution were considered to fire at variable offsets. This permutation method enabled us to control for inherent properties of the task environment or cue position that might bias trace-field position and focus our analyses on cell-specific effects related to the variability of peak-response distances. b) Same as A but for three example memory-trace cells that showed significant offset variability.

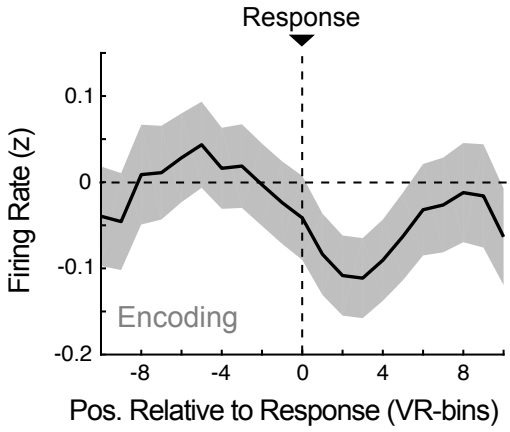

Supplementary Figure 8: **Memory trace cell activity during encoding is not suppressed prior to the object location.** Mean firing rate (z-scored) of all memory-trace cells (black line, $n = 322$ trials) aligned to response location (as in Fig. 5b) for encoding trials. Shading indicates SEM. No bins show significant difference from baseline. This analysis enabled us to examine an alternate explanation for the encoding-retrieval difference we found in memory-trace cell firing rates. Namely, the possibility that memory-trace cells suppress firing rates during encoding trials when an object is visible on the track, similar to either "mismatch cells" in hippocampus or odor-selective suppressive cells in EC[1-3]. Suppression is typically characterized by a decrease in firing prior to stimulus followed by a rebound. This plot shows that memory-trace cells did not show the pattern seen in mismatch cells. *References: 1. Fyhn, M., Molden, S., Hollup, S., Moser, M.-B. & Moser, E. Hippocampal neurons responding to first-time dislocation of a target object. Neuron 35, 555-66 (2002). 2. Xu, W & Wilson D. A. Odor-evoked activity in the mouse lateral entorhinal cortex. Neuroscience 223, 12-20 (2012). 3. Young, B. J., Otto, T., Fox, G. D. & Eichenbaum, H. Memory representation within the parahippocampal region. Journal of Neuroscience 17, 5183-5195 (1997).*

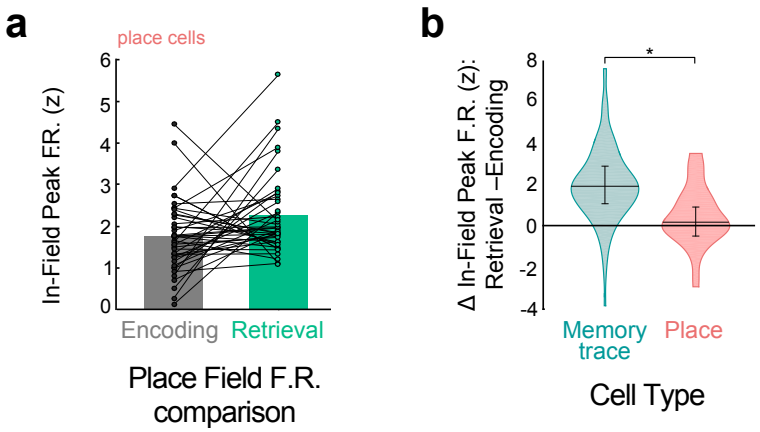

Supplementary Figure 9: **Place cell firing during encoding trials.** a) Comparison of place cells' peak firing rate in field (z-scored) between encoding and retrieval trials, analogous to (Fig. 5e). Circles denote individual fields. Since place cells seemed to show a slight increase in peak in-field firing rate during retrieval trials, we asked how encoding-retrieval differences compared between place cells and memory-trace cells. We thus computed a two-way ANOVA measuring whether in-field firing rate varied as a function of trial type (retrieval vs. encoding), and/or cell type (place cell vs. memory-trace cell). For place cells, we used only the first 12 retrieval trials to match the number of trials used to assess trace fields. We found a significant interaction ($F_{(1,335)} = 24.04$, $p = 0.036$, permutation test), indicating that the increased firing rate we observed for memory trace cells during retrieval was significantly greater than for place cells. b) Violin plots depicting the changes in in-field peak firing between encoding and retrieval trials for memory-trace and place cells (n's$= 43, 45$, respectively). Horizontal line indicates median, upper and lower bounds indicate minima/maxima, and error bars indicate interquartile range (IQR). We used a post-hoc test to directly compare the change between retrieval and encoding in-field firing for place cells and memory-trace cells, and found that place cells exhibited significantly more stable firing fields between retrieval and encoding than memory-trace cells. Asterisk indicates significance from two-sided Mann–Whitney U-test ($z = 5.25$, $p = 1.48 \times 10^{-7}$).

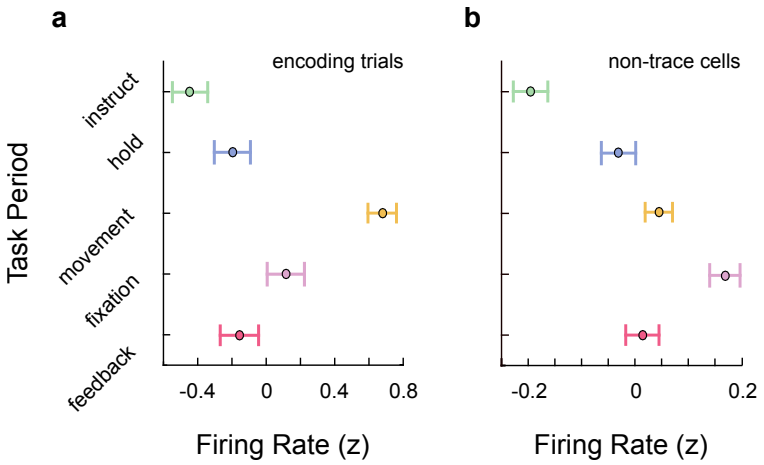

Supplementary Figure 10: **Analysis of firing rate during encoding trials across task periods.** a) Mean firing rates for all memory-trace cells during encoding trials (z-scored) by task period ($n = 332$ trials). Error bars denote SEM. b) Mean firing rate for non-trace cells during retrieval trials by task period ($n = 8472$ trials). Error bars denote SEM.

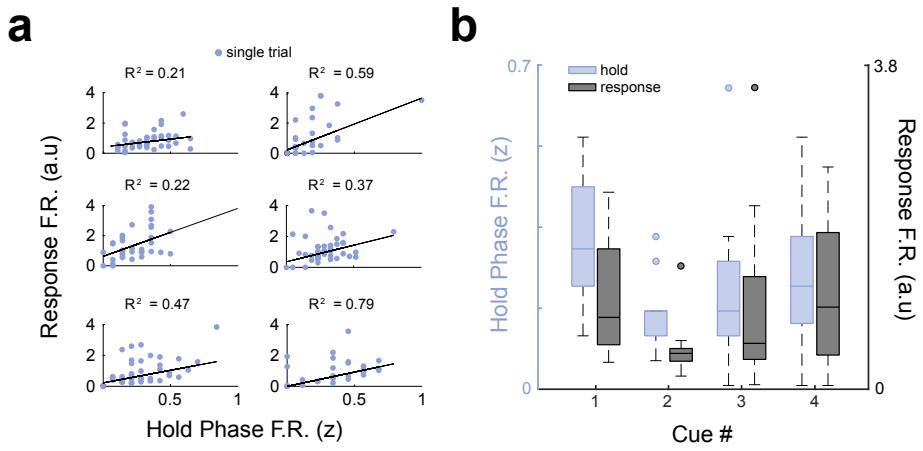

Supplementary Figure 11: **Additional examples of memory-trace cell activity during hold and response periods during retrieval trials.** a) Scatter plots illustrate the relationship between normalized firing rates in the hold and response periods for six representative memory-trace cells across all trials. Line shows the fit from a robust linear regression (similar to Fig. 6b). Each plot depicts 48 retrieval trials, with the exception of the top and bottom plots on the right that depict half sessions of 24 trials. b) Normalized firing rate during hold and response periods for each object cue, for an example EC memory-trace cell (similar to Fig. 6d). Center line indicates median, box limits indicate interquartile range (IQR), whiskers indicate 1.5×IQR ($n = 12$ trials). Circles indicate outliers.

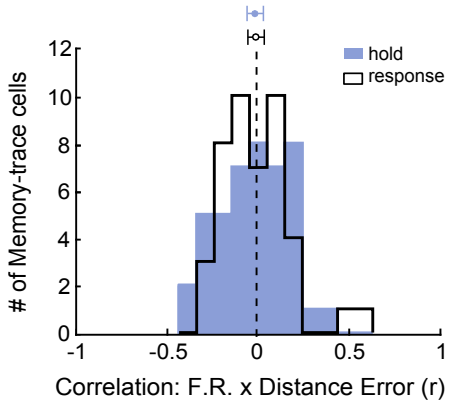

Supplementary Figure 12: **Analysis of the correlation between memory-trace firing rate and distance error during hold and response intervals.** Histograms of Pearson's correlation coefficients between firing rate and distance error for both hold () and response (white) periods ($n = 43$ cells). Black dotted line denotes correlation coefficient of zero. Circles indicate mean, error bars indicate SEM. Both distributions of correlation coefficients are not different from zero (t(42) = 0.73, 0.45, p's= 0.47, 0.66, two-sided t tests), indicating that trial-by-trial memory-trace cell firing rates during both hold and response periods are unrelated to the distance error.

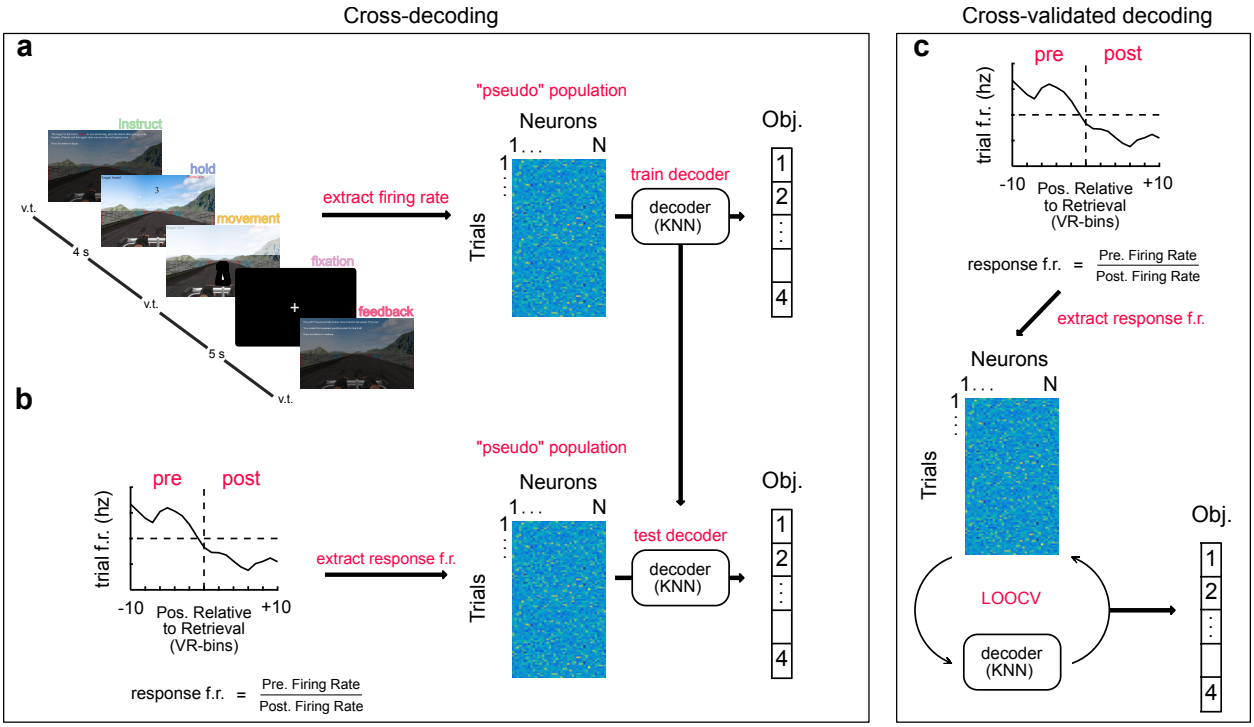

Supplementary Figure 13: **Illustration of the multivariate decoding procedure.** a) Paradigm for cross-decoder training. Pseudopopulations of neural activity were constructed by extracting the activity of cells during the different periods of interest. Decoders were trained on this data using a *k*-nearest-neighbor (KNN) framework to predict the object cue for each trial. b) Paradigm for cross-decoder testing. Response period activity for each trial was computed by normalizing the pre-response firing rate by the post-response firing rate. This measure was extracted for each trial and used as the test set for the decoders trained on each task period. c) Paradigm for cross-validated decoding. We also trained and tested a decoder using just the response period activity. In order to ensure we had separate train–test data, we used leave-one-out cross-validation (LOOCV). The same feature extraction and decoding framework was applied across both task periods.

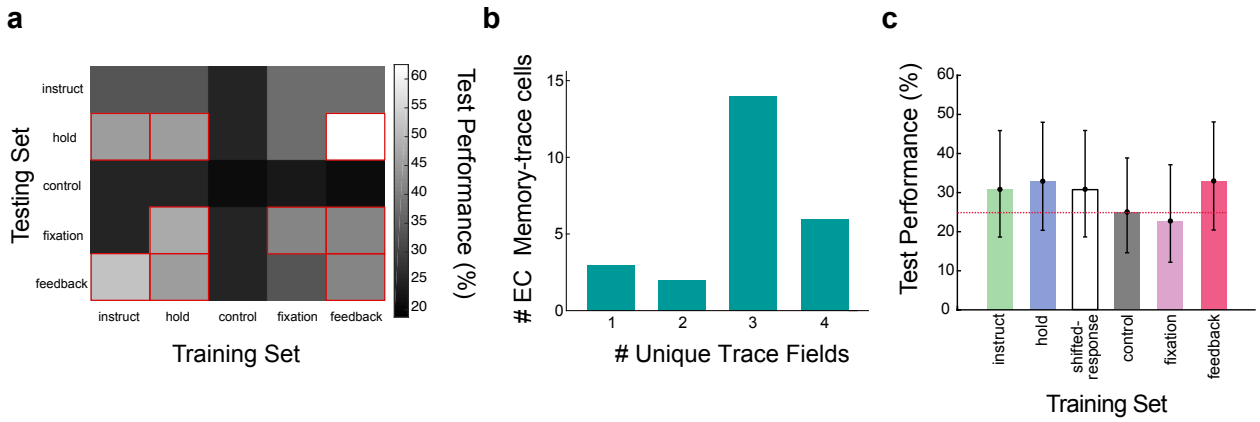

Supplementary Figure 14: **EC memory-trace cell decoding.** a) Matrix of cross-validated decoding accuracy for all train–test combinations of task phases using firing rates from EC memory-trace cells. On-diagonal entries indicate within-condition decoding and off-diagonal entries indicate cross-decoding. Notably, all cross-decoding that tested on the control period performed below significance (chance level at 25%), indicating that the results in Fig. 7a were not an artifact of how we defined the response period. It is also worth noting that training on the feedback period firing rate and testing on the hold period led to the best overall decoding. b) Distribution of the counts of unique trace fields exhibited by memory-trace cells in the EC only. Because EC memory-trace cells primarily had 3+ unique trace-fields, it indicated that our decoding results were driven by dissociable firing rates across different spatial fields rather than being explained by cells with only 1 trace field. c) Results of a control decoding analysis for EC memory-trace cells, using a "shifted" response period closer to non-cued objects ($n = 27$). Individual bars distinguish models that were trained on different task periods, with all models tested on activity during the response period using trial-level cross validation. Bar height denote testing performance, and error bars indicate the 95% confidence interval from a binomial test. Red dotted line denotes chance (25%). We hypothesized that integrating alternate object locations into our decoding would lessen the distinction between different object–location trials and weaken the decoding results. To test this, we defined a "shifted-response" location by computing the firing-rate ratio using a post-response location 6 VR-bins further down the track than the post-response bins used for the original response period—a location that should be closer to a different object location than the current cued object. No cross-decoding yielded significant decoding using the shifted response location, indicating that the spatial bins around the response location were the most informative in decoding the cued object held in memory.

Subject #	# Sessions	Age	Gender	Diagnosis	# Amygdala units	# Hippocampal units	# Entorhinal units	# Cingulate units	# memory-trace cells
R1008	1	55	F	R anterior temporal	0 of (6)	0 of (6)	0 of (0)	0 of (0)	0
R1027	1	48	M	Bi orbitofrontal, R temporal, R insula	1 of (15)	0 of (1)	0 of (0)	0 of (0)	1
R1030	4	23	M	L medial temporal	1 of (21)	0 of (1)	0 of (0)	0 of (0)	1
R1092	3	44	M	Bi medial temporal	0 of (0)	0 of (17)	0 of (0)	0 of (0)	0
R1139	2	19	M	R temporal	0 of (0)	0 of (0)	0 of (0)	2 of (10)	2
R1152	1	20	F	L mesial temporal	0 of (0)	0 of (2)	0 of (0)	5 of (14)	5
R1182	1	40	M	L insula	0 of (0)	0 of (0)	1 of (4)	1 of (3)	2
R1219	1	38	F	L hippocampal head	0 of (0)	0 of (6)	3 of (14)	0 of (0)	3
R1278	3	22	F	R parietal	0 of (0)	0 of (0)	18 of (65)	0 of (0)	18
U0048	1	40	M	L temporal	0 of (10)	1 of (2)	0 of (0)	0 of (0)	1
R1268	1	32	F	R middle temporal gyrus	0 of (0)	0 of (2)	0 of (0)	0 of (0)	0
R1241	1	52	M	Bi medial temporal	1 of (10)	0 of (0)	0 of (0)	0 of (0)	1
R1297	1	24	M	Heterotopia left temporal neocortex	0 of (0)	0 of (3)	0 of (0)	0 of (0)	0
R1299	1	43	M	L hippocampus	0 of (0)	1 of (12)	0 of (0)	0 of (0)	1
R1315	2	22	M	L anterior hippocampus	0 of (0)	0 of (12)	0 of (0)	0 of (0)	0
U0001	1	21	M	R anterior temporal	0 of (0)	1 of (19)	0 of (0)	0 of (0)	1
R1354	2	27	M	L hippocampus	0 of (0)	2 of (14)	0 of (0)	0 of (0)	2
R1362	3	47	M	L amygdala/hippocampus	0 of (0)	0 of (0)	4 of (26)	0 of (0)	4
R1414	1	31	F	R mesial temporal	0 of (0)	0 of (0)	1 of (4)	0 of (0)	1

Supplementary Table 1: **Contribution of subjects and sessions to total cell counts:** Table indicates the total number of memory-trace cells and total cells for each patient, by brain region. The right-most column indicates the number of memory-trace cells observed on unique recording channels across sessions of the task. L: Left, R: Right, Bi: Bilateral.

Control Analysis	% Place Cells	% Memory-trace cells	Place (p)	Memory-trace (p)
Original	*15% (45/299)*	*14% (43/299)*	*NA*	*NA*
One session per patient	16% (31/199)	17% (34/199)	0.87	0.41
Omit seizure onset zone	16% (32/201)	17% (34/201)	0.79	0.44
30 spatial bins	13% (39/299)	15% (46/299)	0.48	0.73
50 spatial bins	10% (31/299)	17% (52/299)	0.09	0.31
GLM	11.0% (33/299)	20.4% (61/299)	0.14	**0.05**

Supplementary Table 2: **Statistical outcomes from control analyses:** Each row of the table indicates the outcome of a different control analysis. We performed χ^2 tests between original results and results of corresponding control analysis (df=1) to assess if proportion of cells categorized as place or memory-trace changed as a function of control conditions. Bold text denotes significance. *Row 1:* The results of the original analysis. *Row 2:* Results of analysis controlling for the dependence of multiple sessions per subject. Several patients contributed multiple sessions of the task, with each session analyzed independently. However, in order to ensure that patients contributing multiple sessions to this study were not confounding our results (Supp. Table 1), we ran control analyses utilizing only the first session recorded from each patient. This controlled for any confounding effect of multiple sessions. *Row 3:* Results of analysis controlling for electrodes placed in epileptic regions. The subject cohort examined in this study has drug-resistent epilepsy. Prior research has supported past work in epileptic cohorts through use of scalp EEG or fMRI[1]. Still, it is important to consider whether electrophysiology research in the epileptic brain is reflective of healthy brain. 31% of the single-units we analyzed were recorded on microwires localized to clinically determined ictal onset zones. To more rigorously control for any confounding effect of epileptic activity, we re-ran all analyses excluding all neurons recorded from these clinically defined ictal onset zones. Our main findings remained unchanged with respect to the proportion of place cells and memory-trace cells. *Rows 4-5:* Results of analysis controlling for the effect of different bin-sizes on spatial firing rate estimates. In order to assess the spatial binning on our results, we calculated the results of our main analyses using 30 and 50 equal sized spatial bins, rather than 40 bins as in our main analyses. The number of place cells and memory-trace cells identified by the ANOVA did not vary significantly as a function of the number of bins. *Row 6:* Results of analysis controlling for potential confounds of using ANOVA for screening of cell responses as "place" or "memory-trace" cells. For our ANOVA analyses, we used a non-parametric permutation method to generate a large number of permutations where observations are permuted within each block. This meant we did not assess significance using a parametric F-test (which is the aspect of the ANOVA generally sensitive to non-normality in the residuals)—rather, we determined our critical statistic against empirically derived null distributions from our permutation testing. Still, to ensure the validity of our statistical categorization of cell responses, we re-did our analysis using a generalized linear model utilizing a Poisson distribution. Setting a rigorous threshold of $p < 0.001$, we found that 61 cells showed a significant interaction (Memory-trace), and 33 showed a main effect of location (Place). Therefore, it is unlikely that our primary finding emerged from the specific analysis used to characterize cell responses, and in fact found more memory-trace cells using this modified approach ($p = 0.05$). *References: 1. Lachaux, J. P., Rudrauf, D., & Kahane, P. Intracranial EEG and human brain mapping. Journal of Physiology-Paris 97, 613-628 (2003).*